Published in the Proceedings of the 16th International Aluminum Alloys Conference (ICAA16) 2018
ISBN: 978-1-926872-41-4
by the Canadian Institute of Mining, Metallurgy & Petroleum

EFFECT OF SURFACE FINISHING PROCEDURES ON CORROSION RESISTANCE OF DMLS-AlSi10Mg_200C ALLOY

*P. Fathi[1], M. Rafieazad[1], M. Mohammadi[2], X. Duan[1], and A.M. Nasiri[1]

[1]Faculty of Engineering and Applied Science, Memorial University of Newfoundland, St. John's, NL, Canada, A1B 3X5
*(*Corresponding author: pfathiahadbe@mun.ca)*

[2]Marine Additive Manufacturing Centre of Excellence (MAMCE), University of New Brunswick, 3 Bailey Drive, P.O. Box 4400, Fredericton, NB, Canada, E3B 5A3

ABSTRACT

Direct metal laser sintering (DMLS) is a metal additive manufacturing technology that creates highly complex components by fusing metal powder into a solid part. In this study, the impact of surface roughness on corrosion resistivity of AlSi10Mg_200C alloy manufactured through DMLS was investigated. The as-printed DMLS-AlSi10Mg _200C alloy was subjected to various surface finishing processes including grinding and sandblasting. The corrosion performance of the surfaces was then evaluated using potentiodynamic polarization testing and electrochemical impedance spectroscopy (EIS) in a 3.5 wt.% NaCl solution to mimic seawater environment. Surface characterization and corrosion morphology of the samples were assessed by Scanning Electron Microscopy (SEM) and Energy Dispersive X-ray (EDX) spectroscopy. The results of this study show that the surface finishing process and the resultant surface roughness has a significant impact on the corrosion resistivity of the DMLS-AlSi10Mg_200C alloy in the seawater environment.

KEYWORDS

Additive manufacturing (AM), AlSi10Mg, Corrosion, Direct metal laser sintering (DMLS), Surface finish.

INTRODUCTION

Direct Metal Laser Sintering (DMLS), also known as Selective Laser Melting (SLM) (Sames, List, Pannala, Dehoff, & Babu, 2016), Laser Beam Melting (LBM), or Laser Metal Fusion (LMF) (Herzog, Seyda, Wycisk, & Emmelmann, 2016), is an additive manufacturing process that utilizes a precise, high-power laser to micro-join powdered metals and alloys layer by layer to form almost fully dense and functional components in three dimensions from the 3D computer-aided design (CAD) data. Complex geometries not possible with conventional manufacturing processes can be readily manufactured with high accuracy using the DMLS process with no need to time-consuming tooling.

The use of light weight Al alloys in modern manufacturing has drastically increased during the last two decades. Among these alloys, Al-Si-Mg alloys are widely used in the automotive, marine, and aerospace industries, because of their high strength and stiffness to weight ratio, low density, and good corrosion resistance (Li, Wang, Jie, & Wei, 2011). In addition, having excellent fluidity, cast ability, and recycling potential have made these alloys a great candidate to be manufactured through DMLS process (Asgari, Baxter, Hosseinkhani, & Mohammadi, 2017). In particular, Al-Si10-Mg alloy is extensively fabricated using the DMLS process primarily due to its reduced coefficient of thermal expansion, leading to low solidification shrinkage and reduced susceptibility to hot cracking during solidification. Also, slight addition of Mg to this alloy (0.20–0.45 wt.% Mg) provides precipitation hardening for the alloy by forming Mg_2Si precipitates upon aging treatments. So far, the major research on this alloy has been focused on the evolution of microstructure and mechanical properties of the alloy processed through various DMLS processing parameters and very little work has been done to understand the corrosion behavior of the DMLS-AlSi10Mg alloy. The impact of microstructure on the corrosion resistivity of additively manufactured AlSi10Mg alloy has been researched in a few recent studies. Cabrini et al. (2016) investigated the impact of different post-heat treatments, *i.e.*, stress relieving and high temperature annealing followed by water quenching, on corrosion behavior of DMLS-AlSi10Mg alloy. The authors demonstrated that the low temperature stress relieving at 537 K, does not affect the susceptibility of the alloy to the selective attack in Harrison solution. However, high temperature annealing at 823 K was reported to promote localized corrosion attack resulted from accelerated galvanic coupling between the course Si particles and surrounding Al matrix. Cabrini et al. (2016) have also evaluated the effect of building direction combined with different surface finishing, including mechanical polishing and shot peening, on corrosion resistivity of DMLS-AlSi10Mg alloy. An improved corrosion resistance was reported for the polished as well as smooth shot-peened surfaces relative to that of the rough as-printed surfaces. Additionally, the authors reported a reduced corrosion resistance of the surfaces parallel to the building direction, which was attributed to the higher density of the melt pool borders containing higher concentration of courser Si particles. The local Volta potential analysis results taken from the melt pool borders reported by Revilla, Liang, Godet, and De Graeve (2017) confirmed a higher potential difference between the Si phase and the α-Al matrix in the border regions with coarser structure, representing a greater driving force for galvanic corrosion. Cabrini et al. (2016) also evaluated the effect of a conversion treatment by short immersion of the AlSi10Mg samples in Ce(III) salt solution. This post-treatment process was not found to be effective in inhibiting corrosion on the as-printed specimen, but was reported to be more effective on polished and pickled surfaces. In a similar study, Leon and Aghion (2017) explored the effect of surface roughness on both general corrosion and corrosion fatigue behaviors of additively manufactured AlSi10Mg processed through SLM, by comparing the as-printed surfaces with the polished ones. An improved corrosion resistance and a higher low cycle corrosion fatigue life span were reported for the polished surfaces over the as-printed ones, associated with increased surface roughness of the as-printed sample. Despite the last two studies available in the literature focused on the impact of surface quality on the corrosion behavior of additively manufactured AlSi10Mg, yet, a comprehensive study is needed to understand the influence of surface morphology on the corrosion behavior of additively manufactured AlSi10Mg alloy. There is also no previous investigation on the corrosion performance of DMLS-AlSi10Mg subjected to the post-grinding or sandblasting process.

This study is aimed to investigate the impact of surface finishing on corrosion performance of AlSi10Mg_200C alloy manufactured through DMLS in seawater environment. Various surface finishing

processes, including grinding and sandblasting, are studied using potentiodynamic polarization testing and electro-chemical impedance spectroscopy (EIS).

EXPERIMENTAL PROCEDURE

Materials

The tests were carried out on 10 × 10 × 10 mm cubes fabricated through DMLS process from a gas atomized AlSi10Mg_200C powder with average particle size of 8.8 ± 7 µm, containing 9–11 wt.% Si, 0.2–0.45 wt.% Mg, less than 0.55 wt.% Fe and Mn, Bal. Al, using an EOS M290 metal 3D printer machine. The DMLS was executed in an argon atmosphere (oxygen content of 0.1%) and elevated building platform temperature of 200°C, to minimize the oxidation and the internal stresses, respectively, during the manufacturing process. Further processing parameters include laser power of 370 W, scanning speed of 1300 mm/s, hatching distance of 190 µm, and powder layer thickness of 30 µm using strip scanning strategy with 67° laser beam rotation between successive layers. The as-fabricated samples provided the as-printed surface condition. Additionally, two other surface conditions were considered in this study. Some of the as-printed samples were subjected to mechanical grinding using 600 grit SiC abrasive paper, provided the ground surface finish samples, and the rest were subjected to sandblasting using a Vaniman micro-abrasive sandblaster, to remove sticky partially melted powders from the surface (sandblasted samples). For this study, 100 µm size aluminum oxide abrasive blasting media was chosen as the abrasive particle. With the distance of 10 mm between the surface and the nozzle, the surfaces were blasted perpendicularly under the pressure of 100 psi. All the samples were ultrasonically cleaned in acetone prior to the electrochemical tests. To assure a complete passivation of specimens after grinding, the specimens were left in air for at least 2 h before subsequent electrochemical testing.

Microscopic Characterization

For microstructural and compositional analysis of the samples, an FEI MLA 650F scanning electron microscope equipped with a high throughput Bruker energy dispersive X-ray (EDX) analytical system was used. To prepare the samples for microscopic analysis, the samples were mounted in an epoxy resin followed by standard grinding and polishing sample preparation procedures. The polished specimens were then etched using Keller's reagent (2.5 cm^3 HNO_3, 1.5 cm^3 HCl, 1 cm^3 HF, and 95 cm^3 H_2O) for 12 s.

Electrochemical Measurements

Potentiodynamic polarization measurements were carried out using an IVIUM CompactStat™ Potentiostat with a three-electrode cell setup in a multiport glass cell at atmospheric pressure based on the ASTM G5-94 standard. The three-electrode cell configuration includes a graphite rod as the counter electrode (CE), a saturated silver/silver chloride (Ag/AgCl, 210±15 mV vs. SHE) as the reference electrode (RE), and the sample as the working electrode. The used electrolyte was 3.5 wt.% NaCl solution and pH 6.5 to simulate seawater corrosion environment at 25°C. After immersion in the solution, the open circuit potential (OCP) was monitored for 1 h for stabilization before the Potentiodynamic polarization test. The scans were performed from −0.3 V to +0.3 V with respect to the OCP with a scanning rate of 0.125 mV/s and an automatic current range between 10 nA and 1 A. To study the corrosion morphology resulted from the potentiodynamic polarization test, the formed corrosion products on the surface were removed by immersing the samples in a concentrated HNO_3 solution (15.8 N) in an ultrasonic bath for 20 min (Ferrer & Kelly, 2001). Electrochemical Impedance Spectroscopy (EIS) measurements were also conducted for immersion times ranging from just immersed to 96 h, every 24 h in the 3.5 wt.% NaCl solution at 25°C, with the amplitude perturbation of ±10 mV (sinusoidal potential signal) with respect to the OCP and a frequency range from 10 kHz to 10 mHz with ten points per decade. The impedance spectra were analyzed using IVIUMSOFT electrochemical analysis software.

RESULTS AND DISCUSSION

Figure 1a shows the as-printed DMLS-AlSi10Mg_200C cubic samples used in this study. The SEM micrographs from the surface of the DMLS-AlSi10Mg_200C at various surface conditions are presented in Figures 1b–d. The as-printed surface (Figure 1b) demonstrates high degree of surface irregularities resulted from the attachment of partially melted powder metal particles to the surface during the DMLS process creating a superficial roughness on the surface in as-printed condition. As shown in Figure 1c, the grinding of the surface using 600 grit SiC abrasive paper, has removed the as-printed surface roughness. The ground surface is characterized by one direction oriented trenches formed during surface preparation. Figure 1d shows the surface morphology of the sandblasted DMLS-AlSi10Mg_200C. Similar to the mechanical grinding, sandblasting also eliminates the partially melted particles from the surface. Meanwhile, it introduces randomly deformed areas on the surface generated as the blasting media impacts the surface. Non-regular peaks and valleys are clearly visible on the sandblasted surface.

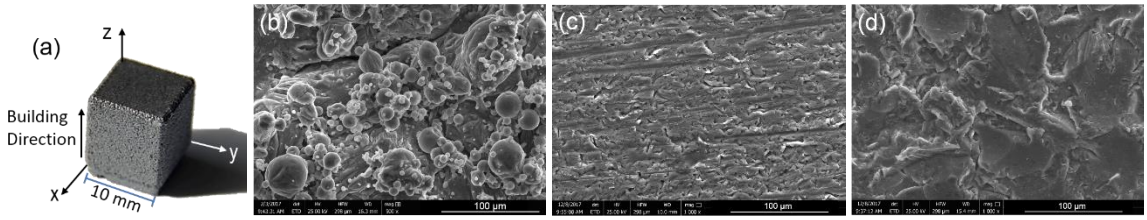

Figure 1. SEM images of DMLS-AlSi10Mg_200C surface in (a) as-printed, (b) ground, and (c) sandblasted conditions

Figure 2 shows the SEM micrographs of the side view of the DMLS-AlSi10Mg_200C (y-z plane), which is investigated through electrochemical testing. The microstructure is characterized by very fine cellular dendritic structure (~ 0.5–2 µm) with non-equilibrium directional solidification features composed of supersaturated α-Al cellular grains and a continuous network of Si phase formed at the intercellular region, resulted from very high cooling rates during solidification. As shown in Figure 2, the cell size changes over the melt pool (MP) from the melt pool center with finer structure (MP-Fine) towards the border with coarser cellular structure (MP-Coarse). A very thin band of heat affected zone (HAZ) (~ 5 µm wide), characterized by broken intercellular network resulted from coarsening of Si phase into idiomorphic crystal, was also detected around each melt pool. This non-uniform cell structure is attributed to the thermal gradient generated by the moving heat source of the DMLS process. The microstructure of additively manufactured AlSi10Mg alloy has been extensively studied in a number of previous works in recent years (Asgari et al., 2017; Cabrini et al., 2016), all confirming that the unique solidification behavior of material during the DMLS process promotes the formation of extremely fine cellular structure.

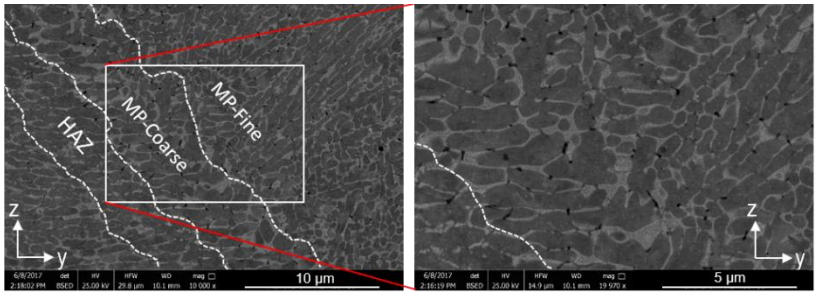

Figure 2. SEM micrographs of DMLS-AlSi10Mg_200C

Figure 3 shows the potentiodynamic polarization behavior of all the specimens with various surface finishing. To allow the stabilization of the OCP, measurements were started 1 h after immersion in 3.5 wt.% NaCl solution. The extracted data from the potentiodynamic polarization measurements, including the

corrosion potentials, polarizations resistance, anodic and cathodic slopes, corrosion current and its density, and corrosion rates are listed in Table 1. The anodic branch of the Tafel plots shown in Figure 3 demonstrates pitting corrosion characteristics, where a slight increase in the applied potential induces a rapid increase in the anodic current, which is more pronounced for the ground and sandblasted DMLS-AlSi10Mg_200C samples. For the as-printed sample, there is a narrow passive region above the corrosion potential (between $E_{corr.}$ and $E_{corr.}$ + 0.05 V), as evidenced by Figure 3. Similar active-like behavior was also observed by Cabrini et al. (2016) and Revilla et al. (2017) for the as-printed additively manufactured AlSi10Mg alloy. On the contrary, a wide passive region was reported for the polished DMLS-AlSi10Mg surfaces (Cabrini et al., 2016). As the surface condition varies from the as-printed surface to the sandblasted one and from the sandblasted to the ground surface, the corrosion rate and corrosion current density increase. Therefore, surface grinding of the as-printed DMLS-AlSi10Mg_200C led to a loss of corrosion resistance by a factor of 5 (see Table 1) in just immersed condition. This is in contrast with the fact that surface roughness and the residual porosities at the surface of the as-printed and sandblasted samples (shown in Figures 1b and 1d) were expected to adversely affect the corrosion resistivity of the alloy by acting as preferential sites for localized corrosion attack, which were removed by the grinding process.

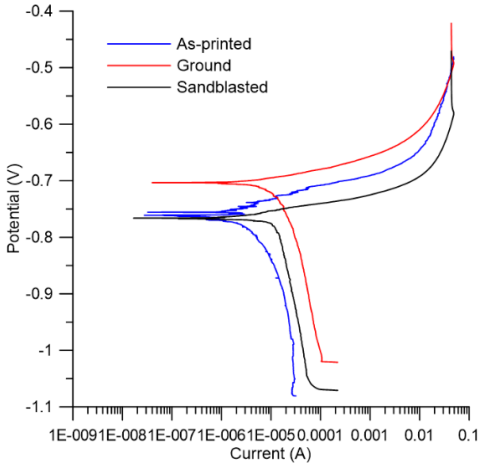

Figure 3. Potentiodynamic polarization curves for the as-printed, ground, and sandblasted AlSi10Mg_200C in 3.5 wt.% NaCl environment

Table 1. Potentiodynamic polarization parameters collected from just immersed DMLS-AlSi10Mg_200C in 3.5 wt.% NaCl solution

Surface finishing	Corrosion potential (V)	Polarization resistance (Ohm)	Anodic slope (V/dec)	Cathodic slope (V/dec)	Corrosion current (A)	Corrosion current density (A/cm^2)	Corrosion rate (mm/year)
As-printed	–0.7710	2955	0.034	0.192	4.266×10^{-6}	1.146×10^{-6}	0.01319
Ground	–0.7058	686.4	0.029	0.350	1.67×10^{-5}	4.775×10^{-6}	0.05504
Sandblasted	–0.7515	438	0.012	0.424	1.202×10^{-5}	3.497×10^{-6}	0.04004

The surface morphology of the samples after potentiodynamic polarization testing followed by the corrosion products removal is shown in Figure 4. The as-printed surface, which demonstrated minimum corrosion rate, confirmed a trivial attack on the surface (Figure 4a) with no indication of pitting corrosion. On the contrary, the ground surface (Figure 4b) experienced a selective attack along the heat affected zone (boundaries of the melt pools), where enrichment of the Si phase and coarsening and breakage of the Si network into an idiomorphic phase were detected (Figure 2b). This has been attributed to the nobility of the Si relative to the α-Al matrix.

Although the sandblasting created a smoother surface finish than the as-printed surface and eliminated the surface porosities (compare Figure 1b with 1d), it has introduced a superficial surface roughness. As shown in Figure 4c, some localized corrosion attack and surface pitting were also noticed on

the sandblasted surface, but not as significant as that of the ground surface. Therefore, the corrosion morphology of the samples and the severity of the corrosion attack are in agreement with the potentiodynamic results, confirming the ground surface to be highly susceptible to localized corrosion attack and the as-printed and the sandblasted surfaces to be more resistant. The improved corrosion resistivity of the as-printed surface was attributed to the coverage of the surface by the accumulated heavily oxidized powder particles with coarse dendritic structures that protects the surface from further oxidation (Fathi, Mohammadi, Duan & Nasiri, 2018).

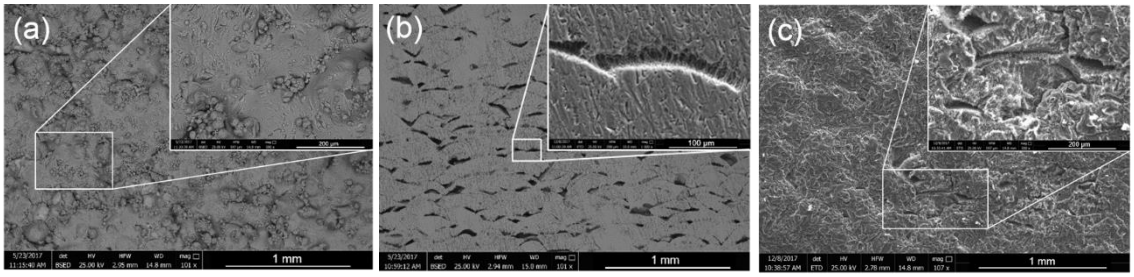

Figure 4. SEM micrographs of the (a) as-printed, (b) ground, and (c) sandblasted DMLS-AlSi10Mg_200C surface after the potentiodynamic polarization test followed by removing the corrosion products.

To investigate integrity of the protective passive layer on the DMLS-AlSi10Mg_200C alloy with different surface finishes after various immersion times, EIS tests were conducted on all samples every 24 h, up to 96 h of immersion in the 3.5 wt.% NaCl solution. The impedance spectra over time are presented in Figure 5 for the as-printed, ground, and sandblasted DMLS-AlSi10Mg_200C, while Figure 6 compiles the effect of surface finishing on the EIS spectrum of the DMLS-AlSi10Mg_200C at constant immersion times. For the samples just immersed in the electrolyte solution (t = 0 h), the Bode plots show significantly lower absolute values of impedance ($|Z|$ Ωcm^2) for the ground DMLS-AlSi10Mg_200C than the as-printed and sandblasted ones at lower frequency range, where the as-printed surfaces show the highest resistance with more than one order of magnitude higher values of $|Z|$ than the sample with the ground surface, confirming a slow kinetic for the corrosion reactions. This higher impedance of the as-printed sample is consistent with the observed corrosion behavior of the samples during potentiodynamic polarization testing (Figure 3), indicating the lowest corrosion rate for the as-printed sample.

The general trend of the impedance with increasing immersion time for the as-printed and sandblasted surfaces (Figures 5a and 5c) was found to be similar confirming a decrease in the modulus of impedance at low frequencies. However, the ground surface showed a different behavior compared to the as-printed and sandblasted ones. As evidenced in Figure 5b, the ground specimen showed an increase of the absolute value of the impedance by two order of magnitude at low frequency with increasing the immersion time from 0 h (just immersed) to 72 h. This increase in the impedance value of the ground surface with the exposure periods exhibited the growth of protective passive film thickness and improvement in the film's resistivity towards diffusion of aggressive ions, through the passive layer (Onofre-Bustamante et al., 2009). After 72 h, the modulus of impedance reaches values slightly lower than 10^5 Ωcm^2, indicating a slower kinetics for corrosion reactions and lower corrosion rates. Longer immersion times (96 h) for the ground surface causes a slight decrease in its absolute value of impedance at low frequencies.

The Bode diagrams (phase angle vs. frequency plots in Figures 5 and 6) of the DMLS-AlSi10Mg with different surface finishing confirmed a typical behavior of passive aluminum characterized by a broad and apparent capacitive peak in the frequency range between 1–100 Hz, which was found to be non-symmetric for the just immersed surfaces, typical of an equivalent circuit having one time constant in this frequency range. For aluminum alloys, such wide peaks are ascribed to superposition of two individual peaks with non-discriminated time constants, one at lower frequency and the other at higher frequency. The peak (capacitive loop) at lower frequency determines the diffusion through the passive layer (corrosion product) and inside the localized corroded areas, whereas the peak at higher frequency can result from the sealing effect of the corrosion film (passive layer) in active areas, such as surface porosities. As opposed to the study

by Cabrini et al. (2016), an inductive behavior was not detected in any of the samples. It is worth noting that for the ground surface, the maximum phase angle has shifted towards the lower frequencies by increasing immersion time, which is another indication for the formation of double layer capacitance and a decrease in active anodic surface area (Lee, Singh, Ismail, & Bhattacharya, 2016).

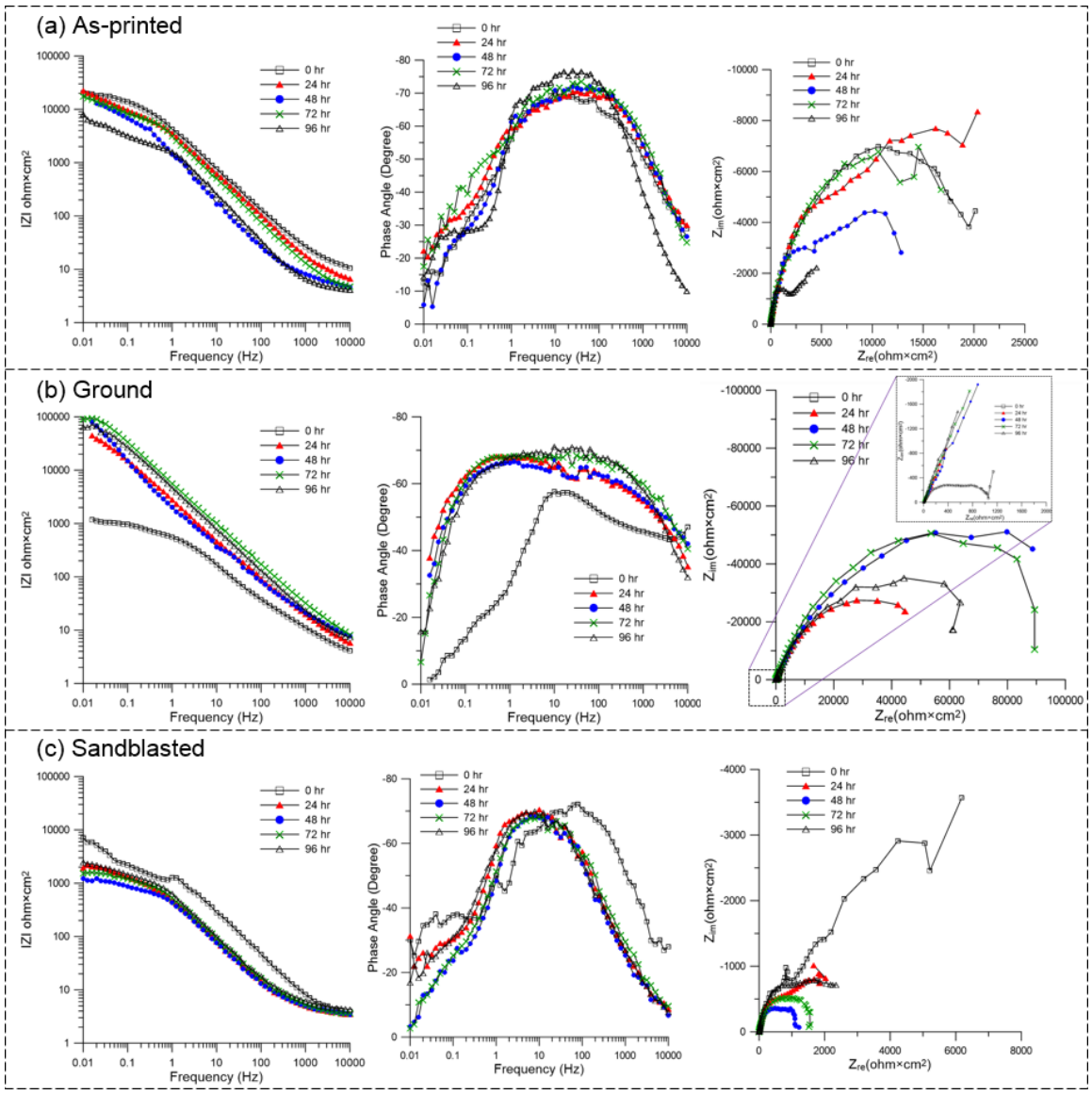

Figure 5. EIS spectra, *i.e.* Z modulus, Bode phase angle plot, and Nyquist plot of DMLS-AlSi10Mg_200C in 3.5 wt.% NaCl solution for the (a) as-printed, (b) ground, and (c) sandblasted surface finish.

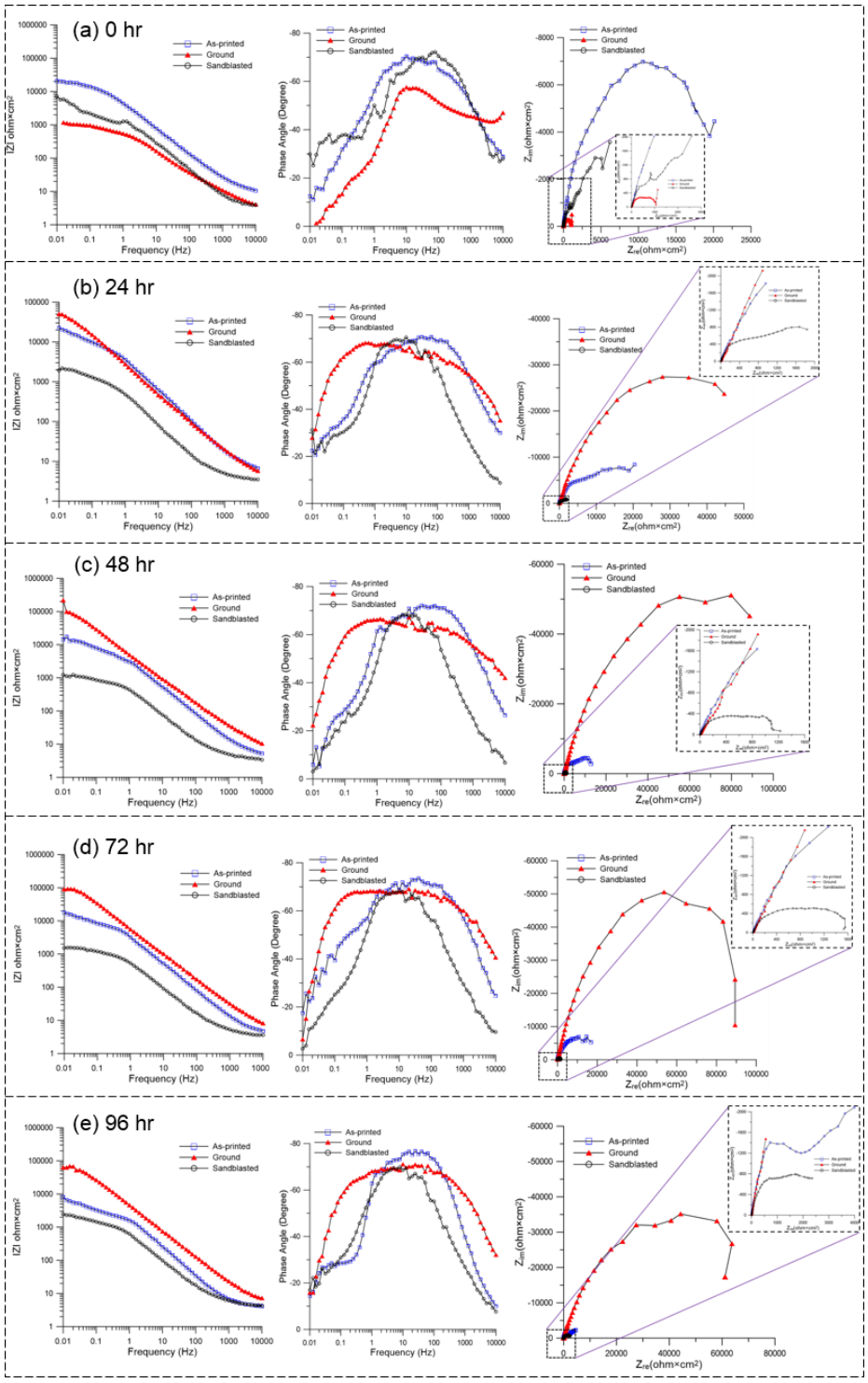

Figure 6. EIS spectrum of DMLS-AlSi10Mg_200C: (a) right after immersion, and after (b) 24 h, (c) 48 h, (d) 72 h, and (e) 72 h of immersion time in 3.5 wt.% NaCl solution.

From the Nyquist plots (Z_{im} vs. Z_{re}) in Figures 5 and 6, the diameter of capacitive arcs for the as-printed and sandblasted samples has decreased considerably with exposure time. In contrast, for the ground

surface (Figure 5c), the dimension of the capacitive arc increases with exposure periods up to 72 h and then decreases for longer immersion times (96 h). For the ground surface, as the exposure time increases, the passivating behavior of the surface enhances as a result of the reduction in the active surface area of the ground surface and the growth of passive layer, leading to an increase in polarization resistance. After 72 h of exposure, the enlargement of the capacitive arc reaches its maximum, exhibiting higher corrosion resistance. This corresponds to the formation of a uniform, dense, and protective passive layer, consistent with the results from the Bode plots. This trend also confirms formation of a double layer capacitance and a lower corrosion rate (Ishizaki, Masuda, & Teshima, 2013).

Corrosion resistance degradation as a result of sandblasting can be explained by the removal of the stable partially melted protective particles from the surface accompanied by the introduced surface roughness. However, in just immersed condition, the sandblasted surface is still covered by a more stable, dense, and protective oxide layer than the ground surface. As shown in Figure 6, after 24 h of immersion, the ground specimens show higher absolute values of impedances at lower frequencies and larger capacitive arcs than the as-printed ones. This modification is even more pronounced when the ground surfaces are compared with the sandblasted ones. This can be ascribed to the more stable passive film that forms on the ground surface after 24 h of immersion in the electrolyte than the as-printed or sandblasted surfaces. Therefore, the corrosion characteristics of DMLS-AlSi10Mg_200C with a ground surface exhibited more passive behavior after 24 h of exposure period than the as-printed or sandblasted ones in 3.5 wt.% NaCl solution. To further investigate the decrease in active anodic behavior of the ground surface by increasing immersion time, the potentiodynamic polarization testing was again conducted after 24 h of immersion. The resultant Tafel plot and the extracted polarization parameters are presented in Figure 7 and Table 2, respectively. After 24 h of immersion, the ground AlSi10Mg_200C sample revealed significantly lower corrosion rate (0.02478 mm/year) than the as-printed (0.0746 mm/year) and sandblasted (0.1236 mm/year) ones. This finding also corroborates the EIS results.

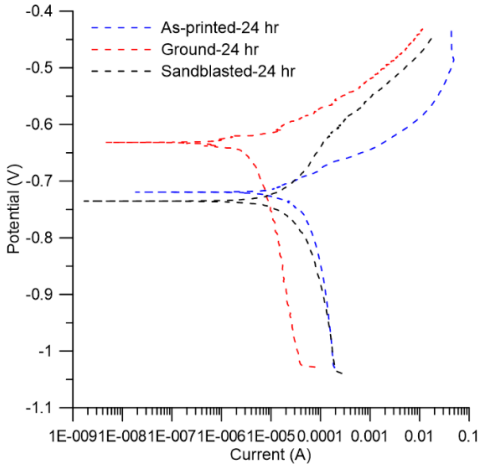

Figure 7. Potentiodynamic polarization curves for the as-printed, ground, and sandblasted AlSi10Mg_200C after 24 h immersion in 3.5 wt.% NaCl environment.

Table 2. Potentiodynamic polarization parameters obtained from DMLS-AlSi10Mg_200C after 24 h immersion in 3.5 wt.% NaCl environment

Surface finishing	Corrosion potential (V)	Polarization resistance (Ohm)	Anodic slope (V/dec)	Cathodic slope (V/dec)	Corrosion current (A)	Corrosion current density (A/cm^2)	Corrosion rate (mm/year)
As-printed	–-0.7070	415.8	0.047	0.397	4.384×10^{-6}	6.48×10^{-6}	0.0746
Ground	–0.6317	3337	0.048	0.461	5.656×10^{-6}	2.154×10^{-6}	0.02478
Sandblasted	–0.7131	1441	0.124	0.288	2.615×10^{-5}	1.074×10^{-5}	0.1236

CONCLUSIONS

The impact of surface finishing, *i.e*. as-printed surface, ground, and sandblasted surfaces, on the corrosion performance of DMLS-AlSi10Mg_200C samples was investigated in 3.5 wt.% NaCl solution at 25°C. At the initial stage of immersion, the as-printed surface demonstrated the lowest corrosion rate accompanied by the lowest corrosion current density and the highest corrosion potential, whereas the ground sample confirmed the highest corrosion rate and corrosion current density and the lowest corrosion potential, which was characterized by a selective attack predominantly at the transition zone (HAZ) between the melt pools, where coarsening of the Si particles were observed. This was attributed to the existence of less protective passive film on the ground surface than the as-printed or sandblasted ones, confirmed by the EIS results. For longer immersion times, *e.g*. after 24 h of immersion in the electrolyte, the corrosion behavior changed and the ground surface demonstrated the highest resistance to the selective attack, which was associated with the formation of a stable, dense, and thick passive film on its surface. Surface porosities and the superficial surface roughness on the as-printed and sandblasted surfaces were found to be more detrimental over time and deteriorated the corrosion performance of the alloy.

ACKNOWLEDGMENTS

The authors wish to acknowledge the support of Natural Sciences and Engineering Research Council of Canada (NSERC), for sponsoring this work. M.M. would like to specially thank New Brunswick Innovation Foundation (NBIF) for providing funding to conduct this research.

REFERENCES

Asgari, H., Baxter, C., Hosseinkhani, K., & Mohammadi, M. (2017). On microstructure and mechanical properties of additively manufactured AlSi10Mg_200C using recycled powder. *Materials Science and Engineering: A*, *707*(September), 148–158. https://doi.org/10.1016/j.msea.2017.09.041

Cabrini, M., Lorenzi, S., Pastore, T., Pellegrini, S., Ambrosio, E. P., Calignano, F., … Fino, P. (2016a). Effect of heat treatment on corrosion resistance of DMLS AlSi10Mg alloy. *Electrochimica Acta*, *206*, 346–355. https://doi.org/10.1016/j.electacta.2016.04.157

Cabrini, M., Lorenzi, S., Pastore, T., Pellegrini, S., Manfredi, D., Fino, P., … Badini, C. (2016b). Evaluation of corrosion resistance of Al – 10Si – Mg alloy obtained by means of Direct Metal Laser Sintering. *Journal of Materials Processing Tech.*, *231*, 326–335. https://doi.org/10.1016/j.jmatprotec.2015.12.033

Cabrini, M., Lorenzi, S., Pastore, T., Pellegrini, S., Pavese, M., Fino, P., … Manfredi, D. (2016c). Corrosion resistance of direct metal laser sintering AlSiMg alloy. *Surface and Interface Analysis*, *48*(8), 818–826. https://doi.org/10.1002/sia.5981

Fathi, P., Mohammadi, M., Duan, X., Nasiri, A. M. (2018). A Comparative study on corrosion and microstructure of direct metal laser sintered AlSi10Mg_200C and die cast A360.1 aluminum. *Journal of Materials Processing Technology*, *Submitted*.

Ferrer, K. S., & Kelly, R. G. (2001). Comparison of Methods for Removal of Corrosion Product from AA2024-T3. *Corrosion*, *57*(2), 110–117.

Herzog, D., Seyda, V., Wycisk, E., & Emmelmann, C. (2016). Additive manufacturing of metals. *Acta Materialia*, *117*, 371–392. https://doi.org/10.1016/j.actamat.2016.07.019

Ishizaki, T., Masuda, Y., & Teshima, K. (2013). Composite film formed on magnesium alloy AZ31 by chemical conversion from molybdate/phosphate/fluorinate aqueous solution toward corrosion protection. *Surface and Coatings Technology*, *217*(Supplement C), 76–83.

Lee, H.-S., Singh, J. K., Ismail, M. A., & Bhattacharya, C. (2016). Corrosion Resistance Properties of Aluminum Coating Applied by Arc Thermal Metal Spray in SAE J2334 Solution with Exposure Periods. *Metals*, *6*(3).

Leon, A., & Aghion, E. (2017). Effect of surface roughness on corrosion fatigue performance of AlSi10Mg alloy produced by Selective Laser Melting (SLM). *Materials Characterization*, *131*(June), 188–194.

Li, B., Wang, H., Jie, J., & Wei, Z. (2011). Effects of yttrium and heat treatment on the microstructure and tensile properties of Al–7.5Si–0.5Mg alloy. *Materials & Design*, *32*(3), 1617–1622.

Onofre-Bustamante, E., Domínguez-Crespo, M. A., Torres-Huerta, A. M., Olvera-Martínez, A., Genescá-Llongueras, J., & Rodríguez-Gómez, F. J. (2009). Characterization of cerium-based conversion coatings for corrosion protection of AISI-1010 commercial carbon steel. *Journal of Solid State Electrochemistry*, *13*(11), 1785–1799. https://doi.org/10.1007/s10008-009-0871-9

Revilla, R. I., Liang, J., Godet, S., & De Graeve, I. (2017). Local corrosion behavior of additive manufactured AlSiMg alloy assessed by SEM and SKPFM. *Journal of The Electrochemical Society*, *164*(2), C27–C35. https://doi.org/10.1149/2.0461702jes

Sames, W. J., List, F. A., Pannala, S., Dehoff, R. R., & Babu, S. S. (2016). The metallurgy and processing science of metal additive manufacturing. *International Materials Reviews*, *61*(5), 315–360.